

Atomic Pt-Catalyzed Heterogeneous Anti-Markovnikov C–N Formation: Pt₁⁰ Activating N–H for Pt₁^{δ+}-Activated C=C Attack

Xiaodan Ma, Zhe An, Hongyan Song, Xin Shu, Xu Xiang, and Jing He*

Cite This: *J. Am. Chem. Soc.* 2020, 142, 9017–9027

Read Online

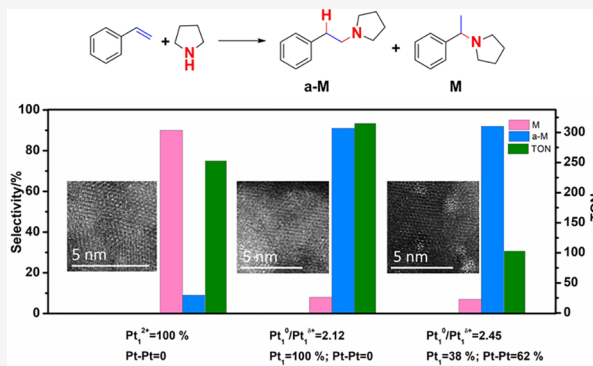
ACCESS |

Metrics & More

Article Recommendations

Supporting Information

ABSTRACT: C–N formation is of great significance to synthetic chemistry, as N-containing products are widely used in chemistry, medicine, and biology. Addition of an amine to an unsaturated carbon–carbon bond is a simple yet effective route to produce new C–N bonds. But how to effectively conduct an anti-Markovnikov addition with high selectivity has been a great challenge. Here, we proposed a strategy for highly regioselective C–N addition via hydroamination by using supported Pt. It has been identified that atomic-scale Pt is the active site for C–N addition with Pt₁²⁺ for Markovnikov C–N formation and atomic Pt (Pt₁^{δ+} and Pt₁⁰) contributing to anti-Markovnikov C–N formation. A selectivity of up to 92% to the anti-Markovnikov product has been achieved with atomic Pt in the addition of styrene and pyrrolidine. A cooperating catalysis for the anti-Markovnikov C–N formation between Pt₁^{δ+} and Pt₁⁰ has been revealed. The reaction mechanism has been studied by EPR spectra and in situ FT-IR spectra of adsorption/desorption of styrene and/or pyrrolidine. It has been demonstrated that Pt₁⁰ activates amine to be electrophilic, while Pt₁^{δ+} activates C=C by π -bonding to make β -C nucleophilic. The attack of nucleophilic β -C to electrophilic amine affords the anti-Markovnikov addition. This strategy proves highly effective to a variety of substrates in anti-Markovnikov C–N formation, including aromatic/aliphatic amines reacting with aromatic olefins, aromatic/aliphatic olefins with aromatic amines, and linear aliphatic olefins with secondary aliphatic amines. It is believed that the results provide evidence for the function of varied chemical states in monatomic catalysis.



1. INTRODUCTION

Supported Pt catalysts have been attracting significant attention for decades^{1–3} due to their wide application in the petrochemical industry (including catalytic re-forming⁴ and hydrogenation⁵/dehydrogenation⁶) and the fine chemical field (including C–O conversion^{7,8} and carbonylation⁹). A number of reactions, including the formation or breakage of C–C, N–N, and C–O, have been found as being structure-sensitive,^{4,10–12} so well-dispersed Pt in ensembles,^{1–4} clusters,^{13,14} or even single atoms^{13–17} have been required. Supported atomic Pt has been of interest in the past 10 years due to its impressive activity in CO oxidation,¹⁴ selective hydrogenation of nitro-compounds,¹⁵ CO₂ hydrogenation,¹⁶ or methane conversion.¹⁷ However, the application of atomic Pt in the catalytic synthesis of commodity chemicals and staple compounds needs more attention.

The C–N formation is an important strategy to produce N-containing organic compounds, usually accomplished only with homogeneous catalysts.^{18–23} Hydroamination, one mild and atom-economic route for direct production of C–N bonds by the addition of an amine to an unsaturated carbon–carbon bond, is of particular significance and has been focused on for decades.^{22,23} Pt(II) has been revealed as the most active catalyst since a turnover number (TON) of 250 in 72 h has

been afforded in the hydroamination of ethylene with 2-chloroaniline by using a PtBr₂/3CF₃SO₃H system as catalyst and *n*Bu₄PX (X = halide) as activator.²⁴ The addition of nitrogen to allenes has been reported to be accomplished with supported Pt nanoparticles.²⁵ But the effective catalysis of supported Pt nanoparticles needs a treatment of Pt with oxidants, and so the active sites are actually Pt(II) sites.²⁵ The stoichiometric reaction of secondary amines, such as diethylamine, on coordinated olefins in *cis*- or *trans*-[Pt(C₂H₄)C₁₂L] has been known for a long time.²⁶ With the promotion of phosphorus ligands (PPh₃,^{27,28} phosphonium halides,²⁹ or alkyl phosphites³⁰) or the aid of AgOTf,³¹ Pt(II) or Pt(IV) complexes have been demonstrated effective for intra- or intermolecular hydroamination. The above Pt-catalyzed C–N addition is based on N–H bond activation followed by olefin

Received: March 17, 2020

Published: April 21, 2020



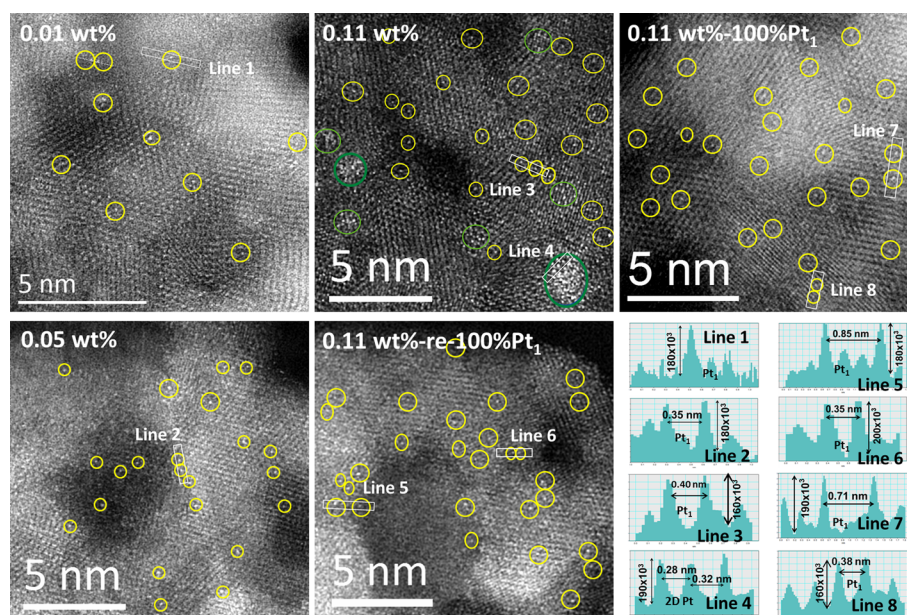


Figure 1. HAADF-STEM images and brightness intensity profiles of Pt for 0.01 wt % Pt/Zn(Al)O, 0.05 wt % Pt/Zn(Al)O, 0.11 wt % Pt/Zn(Al)O, 0.11 wt % Pt/Zn(Al)O-re-100%Pt₁, and 0.11 wt % Pt/Zn(Al)O-100%Pt₁. The Pt sites with a thickness of the Pt layer around atomic scale and a distance between Pt atoms much larger than Pt–Pt bonds (0.28 nm) are atomically dispersed Pt (Pt₁). The Pt sites with a thickness of the Pt layer around atomic scale and a distance between Pt atoms of ca. Pt–Pt bonds (0.28 nm) are 2D Pt clusters. Yellow circles: Pt₁ atoms; green circles: 2D Pt clusters.

insertion or the nucleophilic attack of an amine to a coordinated olefin.^{27–31}

For the C–N formation via hydroamination, the regioselectivity control is vital and anti-Markovnikov addition is a great challenge.^{22,23} Few catalytic systems have been reported to be effective for anti-Markovnikov hydroamination.^{32–37} The first intermolecular anti-Markovnikov hydroamination has been achieved between a nonactivated aromatic olefin and morpholine with cationic rhodium complexes as catalyst.³² Then Au(I),³³ Ru(II),^{34,35} or Ir(III)^{36,37} complexes have been reported to catalyze anti-Markovnikov addition. It is interesting that under the promotion of electron-deficient ligands (N-heterocyclic carbene or chelating bisphosphine),^{32,33} the regioselectivity for the hydroamination on Rh(I) and Au(I) complexes changes to anti-Markovnikov from Markovnikov.^{38–41} The C–N addition on Rh(I) is based on N–H bond activation followed by olefin insertion, but the regiochemically controlling element is still not clear.^{32,38,39} For Au(I), the C–N addition is achieved by nucleophilic attack of an amine to a coordinated olefin,^{33,40} and the regiocontrol to anti-Markovnikov is ascribed to the sp hybridization of the substrate (alkylidenecyclopropanes).³³ More interesting is that Ru(I)^{42,43} or Ir(I)^{39,44} has been reported to catalyze Markovnikov C–N addition, while Ru(II)^{34,35} and Ir(III)^{36,37} complexes are found to be active for anti-Markovnikov C–N addition, although chelating ligands and Brønsted acid (TfOH) are required for Ru(II)^{34,35} and indispensable thiol as a proton donor and visible light conditions are required for Ir(III).^{36,37} For Ru(I)^{42,43} and Ir(I),⁴⁴ the Markovnikov C–N addition is achieved by amine activation, followed by alkene insertion into the Ru–N or Ir–N bond. Ru(II)^{34,35} complexes have been suggested to catalyze the anti-Markovnikov hydroamination by attack of amine to the π -arene intermediates. The Ir(III) photocatalyst^{36,37} has been proposed to oxidize amine/amide to its corresponding

aminium radical cation, and then this electrophilic N-centered radical attacks an olefin to furnish a new C–N bond.

Despite all the impressive progress in homogeneous catalysis, more intensive efforts are demanded to develop (1) heterogeneous catalysis for anti-Markovnikov hydroamination of olefins and (2) a highly active heterogeneous catalyst for anti-Markovnikov hydroamination. Although Pt(II) or Pt(IV) has been reported as the most active site for hydroamination, no anti-Markovnikov C–N addition has been achieved with Pt(II) or Pt(IV) sites. The regioselective 1,2-insertion of acrylonitrile into the Pt–N bond of *cis*-[PtH(NHPh)(PEt₃)₂] affords anti-Markovnikov product,^{45,46} but it is a stoichiometric reaction. Here this work reports a highly active and selective heterogeneous hydroamination with supported Pt as catalyst. Atomic Pt has been revealed to effectively catalyze anti-Markovnikov C–N formation, affording a selectivity of up to 92% to anti-Markovnikov product in the hydroamination of styrene with pyrrolidine. It is an original demonstration of (1) heterogeneous catalysis for C–N formation via anti-Markovnikov hydroamination of olefins; (2) Pt-catalyzed anti-Markovnikov hydroamination; and (3) a cooperation between varied metal sites (Pt₁^{δ+} and Pt₁⁰) in monatomic Pt catalysis. The supported Pt reported here (Pt/Zn(Al)O) has been prepared simply by calcination under a H₂ atm of Pt-loaded Zn and Al-containing layered double hydroxides (ZnAl-LDHs). LDHs have proved to be excellent precursors for supported Pt.^{47–49} This strategy is also effective for the anti-Markovnikov addition of aromatic olefins with aromatic/aliphatic amines, and linear aliphatic olefins with secondary aliphatic amines.

2. RESULTS AND DISCUSSION

2.1. Preparation and Characterization of Pt/Zn(Al)O.

Zn(Al)O-supported Pt (Pt/Zn(Al)O) was produced in this work by reduction of Pt-loaded ZnAl-LDHs. ZnAl-LDHs used

for impregnation of Pt in this work were prepared by a pH-constant co-precipitation method.^{50,51} The (003), (006), (009), (015), (018), (110), and (113) reflections characteristic of hydrocalcite structure⁵⁰ are clearly observed in the X-ray diffraction (XRD) patterns (Figure S1). Pt²⁺ was introduced in varied loading by incipient wetness impregnation⁵² of ZnAl-LDHs with positively charged Pt precursor ($[(\text{NH}_3)_4\text{Pt}]^{2+}$). The hydrocalcite structure is well retained according to the XRD patterns (Figure S1). Calcination of Pt-impregnated ZnAl-LDHs under a reduction atmosphere produced Pt/Zn(Al)O in varied Pt loading (Table S1). Only a ZnO-like phase is observed for all Pt/Zn(Al)O (Figure S2). In the high-angle annular dark-field scanning transmission electron microscopic (HAADF-STEM) images, only atomic-scale Pt (Pt₁) can be observed in 0.01 wt % Pt/Zn(Al)O and 0.05 wt % Pt/Zn(Al)O, while Pt₁ (76%) coexists with 2D Pt clusters (single-layered Pt–Pt, 24%) for 0.11 wt % Pt/Zn(Al)O (Figure 1). With Pt loading further increasing to 0.30, 1.01, and 2.12 wt % (Figure S3), 3D Pt ensembles (two- or multilayered Pt–Pt) emerge in addition to the Pt₁ and 2D clusters, and the ratio of Pt₁ to Pt–Pt sites has been determined as 47:53, 38:62, and 30:70 (Figure S3). No atomic-scale Pt but Pt clusters and particles (Pt–Pt, 100%) are observed for 5.05 wt % Pt/Zn(Al)O (Figure S4). The dispersion of Pt, determined by the hydrogen–oxygen titration (HOT) method⁵³ (Table S1), is consistent with that estimated from the HAADF-STEM images.

According to the in situ Fourier-transformed infrared (FT-IR) spectra of CO adsorption (Figure 2A), the atomic-scale Pt in 0.01 wt % Pt/Zn(Al)O is all positively charged (the adsorption at 2085 cm⁻¹ assigned^{14,54} to linearly adsorbed CO on atomic-scale Pt^{δ+}), while the atomic-scale Pt in 0.05 wt % Pt/Zn(Al)O consists of both Pt^{δ+} (linearly adsorbed CO at

2055 cm⁻¹ on atomic-scale Pt^{δ+}) and Pt⁰ sites (linearly adsorbed CO at 2020 cm⁻¹ on atomic-scale Pt⁰). The red shift from 2085 cm⁻¹ for the CO adsorbed on Pt^{δ+} to 2055 cm⁻¹ suggests that the electron density of Pt^{δ+} increases with Pt loading increasing from 0.01 to 0.05 wt %. On further increasing the Pt loading (0.11 to 2.12 wt %), the adsorption on Pt⁰ (the band at 2020 cm⁻¹) gets obvious (for 0.11 wt % Pt) and predominates over Pt^{δ+} (for 0.30 to 2.12 wt % Pt). The band to bridge-bound CO on the Pt cluster support (at 1975 cm⁻¹)^{55,56} emerges at 0.11 wt % Pt loading and becomes marked (red shift to 1945 cm⁻¹ with the emergence of 3D Pt ensembles) at 0.30 wt % Pt loading. At 0.30 wt % Pt loading, the adsorption on Pt–Pt sites^{14,55,56} emerges, consistent with the HAADF-STEM observations of 3D Pt ensembles (Figure 1 and Figure S3).

In the electron paramagnetic resonance (EPR) spectra (Figure 2B), except for the EPR signal resulting from oxygen vacancies⁵⁷ in the Zn(Al)O support ($g = 2.003$), no other signal is observed for 0.01 wt % Pt/Zn(Al)O, indicating the atomic-scale Pt^{δ+} in 0.01 wt % Pt/Zn(Al)O was actually Pt₁²⁺. The EPR signal assigned to Pt ($g = 1.971$) emerges at 0.05 wt % Pt loading and gets more visible for 0.30 wt % Pt/Zn(Al)O, suggesting that the atomic-scale Pt was Pt₁⁰ or Pt₁^{δ+} in these cases. The EPR observations well account for the red shift of CO adsorption from 2085 to 2055 cm⁻¹ in the FT-IR spectra with Pt loading increasing from 0.01 to 0.05 wt % (Figure 2A). For 5.05 wt % Pt/Zn(Al)O, the signal at $g = 1.971$ disappears because of the formation of a Pt–Pt bond at 100%. According to literature observations,⁵⁸ atomic-scale Pt could coordinate with lattice oxygen sites or be located at lattice Zn(Al) sites, as observed here in the HAADF-STEM images (Figure S5). The Pt₁^{δ+} results from the electron transfer from Pt to O atoms, while the Pt₁⁰ binding to the Zn(Al) sites remains neutral. The ratio of Pt₁⁰ to Pt₁^{δ+} in surface Pt is determined as 0.33, 0.89, 2.03, 2.45, and 3.55 for 0.05, 0.11, 0.30, 1.01, and 2.12 wt % Pt/Zn(Al)O, according to the quantitative estimation following the reference method.⁵⁹

2.2. Catalytic Hydroamination on Pt/Zn(Al)O. **2.2.1. Active Pt Sites for C–N Formation.** Pt/Zn(Al)O has then been used as a catalyst for hydroamination. In the addition of styrene and pyrrolidine (Table 1), 0.01 wt % Pt/Zn(Al)O (Table 1, entry 1) affords a TON of 253 in 8 h. No conversion of styrene and pyrrolidine has occurred on Zn(Al)O. The TON increases to 265 on 0.05 wt % Pt/Zn(Al)O (Table 1, entry 2) and then decreases to 225, 156, 103, and 49 for 0.11, 0.30, 1.01, and 2.12 wt % Pt/Zn(Al)O (Table 1, entries 3–6). The TON displays a rapid decrease with decreasing Pt₁ ratio or increasing Pt–Pt site fraction (Figure S6), indicating that Pt₁ sites are the active sites for C–N addition. The 5.05 wt % Pt/Zn(Al)O was found to be totally inactive for the reaction (Table 1, entry 7), confirming that Pt–Pt sites are not active for the reaction.

To define the active sites for C–N formation, 0.11 wt % Pt/Zn(Al)O has been further treated to tailor the ratio of Pt₁ in total Pt to be 100% (0.11 wt % Pt/Zn(Al)O-re-100% Pt₁, Figure 1) or 14% (0.11 wt % Pt/Zn(Al)O-re-14% Pt₁, Figure S7). Or in another way, 0.11 wt % Pt/Zn(Al)O has been prepared directly to tailor Pt sites as Pt₁ at 100% (0.11 wt % Pt/Zn(Al)O-100% Pt₁), 18% (0.11 wt % Pt/Zn(Al)O-18% Pt₁), or 0 (0.11 wt % Pt/Zn(Al)O-0Pt₁) (Figures 1 and S8). According to the in situ FT-IR spectra of CO adsorption (Figure 2A), for either 0.11 wt % Pt/Zn(Al)O-re-100% Pt₁ or 0.11 wt % Pt/Zn(Al)O-100% Pt₁, Pt₁⁰ (the band at 2020

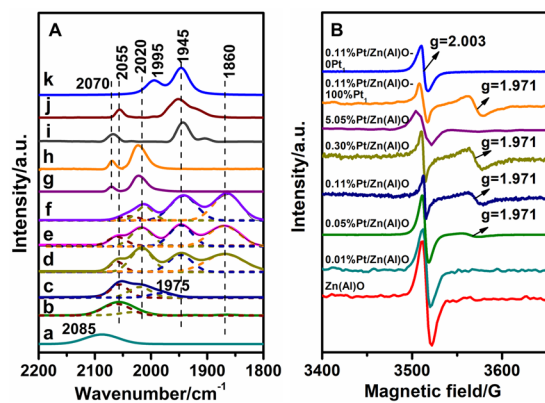
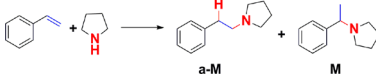


Figure 2. (A) In situ FT-IR spectra of CO adsorbed on (a) 0.01 wt % Pt/Zn(Al)O, (b) 0.05 wt % Pt/Zn(Al)O, (c) 0.11 wt % Pt/Zn(Al)O, (d) 0.30 wt % Pt/Zn(Al)O, (e) 1.01 wt % Pt/Zn(Al)O, (f) 2.12 wt % Pt/Zn(Al)O, (g) 0.11 wt % Pt/Zn(Al)O-re-100%Pt₁, (h) 0.11 wt % Pt/Zn(Al)O-re-100%Pt₁, (i) 0.11 wt % Pt/Zn(Al)O-re-14%Pt₁, (j) 0.11 wt % Pt/Zn(Al)O-18% Pt₁, and (k) 0.11 wt % Pt/Zn(Al)O-0Pt₁. The adsorption bands at 2055–2085 and 2000–2030 cm⁻¹ are ascribed respectively to linearly adsorbed CO on atomic-scale Pt^{δ+} sites^{14,54} and Pt⁰ sites in atomic-scale Pt or very small Pt clusters.¹⁴ The adsorption bands at 1950–1975 and 1860 cm⁻¹ can be assigned to bridge-bound CO on the Pt cluster support^{14,55,56} and Pt–Pt sites.^{14,55,56} (B) EPR spectra for Zn(Al)O and Pt-loaded Zn(Al)O. Signal at $g = 2.003$ is supposed to come from O²⁻ vacancies on the Zn(Al)O surface, based on the observation for ZnO in the literature.⁵⁷

Table 1. Pt-Catalyzed C–N Addition of Styrene and Pyrrolidine^a


entry	catalyst	Pt ₁ ratio in surface Pt ^b	Pt ₁ ⁰ /Pt ₁ ^{δ+} ^c	sel./% ^f		TON ^d	TON _{Pt₁} ^e
				a-M	M		
1	0.01 wt % Pt/Zn(Al)O	1.00	0 (Pt ₁ ⁰ /Pt ₁ ²⁺)	9 (8)	90 (90)	253	253
2	0.05 wt % Pt/Zn(Al)O	1.00	0.33	55 (53)	43 (45)	265	265
3	0.11 wt % Pt/Zn(Al)O	0.76	0.89	85 (86)	13 (12)	225	293
4	0.30 wt % Pt/Zn(Al)O	0.47	2.03	90 (92)	8 (7)	156	331
5	1.01 wt % Pt/Zn(Al)O	0.38	2.45	92 (93)	7 (5)	103	271
6	2.12 wt % Pt/Zn(Al)O	0.30	3.55	93 (91)	6 (8)	49	165
7	5.05 wt % Pt/Zn(Al)O	0				0	
8	0.11 wt % Pt/Zn(Al)O-re-100% Pt ₁	1.00	2.12	91	8	315	315
9	0.11 wt % Pt/Zn(Al)O-re-14% Pt ₁	0.14	0.08	37	62	31	221
10	0.11 wt % Pt/Zn(Al)O-100% Pt ₁	1.00	1.78	90	8	327	327
11	0.11 wt % Pt/Zn(Al)O-18% Pt ₁	0.18	0.19	36	61	46	258
12	0.11 wt % Pt/Zn(Al)O-0Pt ₁	0				0	

^aReaction conditions: styrene (0.6 mmol), pyrrolidine (0.3 mmol), catalysts (exposed Pt = 0.067 mol %), and solvent (isopropanol 1.5 mL) in a Schlenk tube, $T = 60\text{ }^{\circ}\text{C}$, $t = 8\text{ h}$. ^bPt–Pt and total Pt₁ were estimated from HAADF-STEM images; Pt–Pt + Pt₁ = surface Pt. ^cPt₁^{δ+} was estimated from in situ FT-IR of CO adsorption; Pt₁⁰ + Pt₁^{δ+} = Pt₁. ^dTON was calculated based on the number of surface Pt sites. The number of surface Pt sites was estimated from the Pt dispersion (D_{Pt} in Table S1). ^eTON_{Pt₁} was based on Pt₁ sites. ^fThe numbers in parentheses are reproduced data.

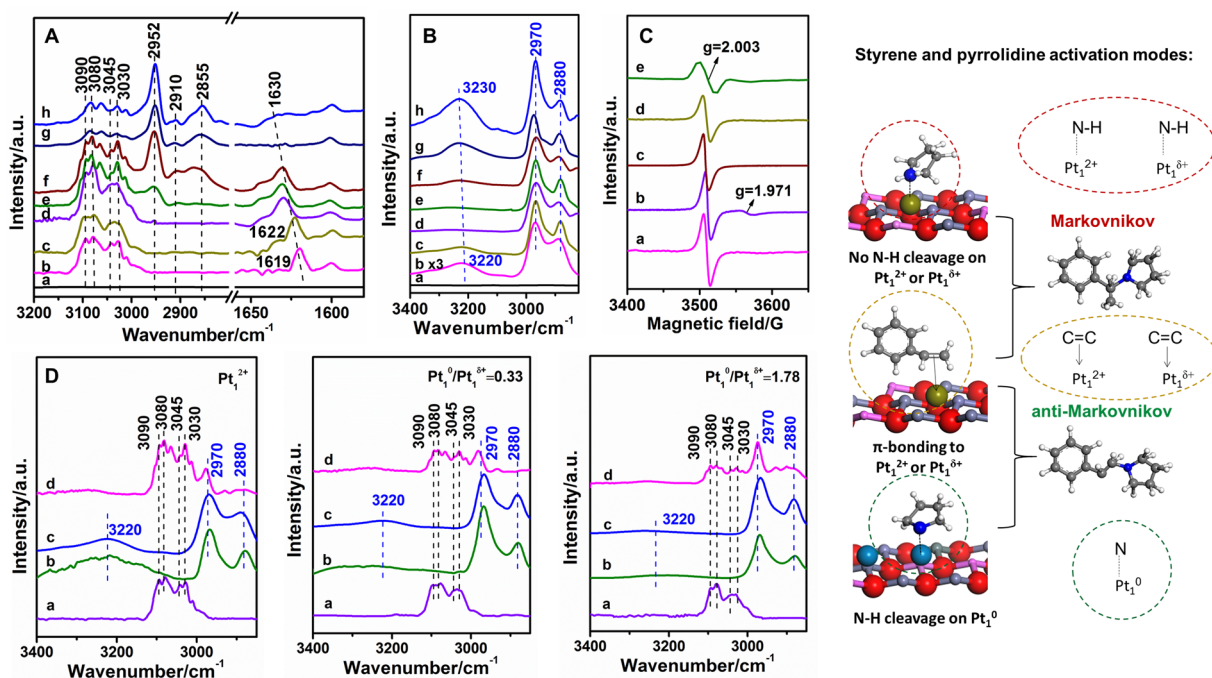


Figure 3. In situ FT-IR spectra of (A) styrene and (B) pyrrolidine adsorption on (a) Zn(Al)O and Pt/Zn(Al)O with Pt present as (b) Pt₁²⁺, (c) Pt₁ at 100% with a Pt₁⁰/Pt₁^{δ+} ratio of 0.33, (d) Pt₁ at 100% with a Pt₁⁰/Pt₁^{δ+} ratio of 1.78, (e) Pt₁ at 47% with a Pt₁⁰/Pt₁^{δ+} ratio of 2.03, (f) Pt₁ at 38% with a Pt₁⁰/Pt₁^{δ+} ratio of 2.45, (g) 2D clusters and 3D ensembles, and (h) 3D ensembles and particles. The adsorption bands around 3030 and 3080 cm⁻¹ are assigned, according to previous reports,⁶⁰ to the C–H stretching vibrations of the benzene ring. The bands at 1605–1642 cm⁻¹ can be assigned to C=C stretching vibrations.^{49,61,62} The bands around 3045 and 3090 cm⁻¹ can be assigned to C–H stretching vibrations of CH=CH₂,⁶² and the bands at 2825–2960 cm⁻¹ are assigned to CH₂ and C–H stretching vibrations of di-σ-bonded olefins.^{63–65} The bands at 2864–2995 cm⁻¹ are assigned to the CH₂ stretching vibration of adsorbed amine,⁶⁶ and those at 3150–3310 cm⁻¹ can be assigned to N–H stretching vibration.^{67,68} (C) EPR spectra for pyrrolidine-adsorbed Pt/Zn(Al)O with Pt present as (a) Pt₁²⁺, (b) Pt₁ at 100% with a Pt₁⁰/Pt₁^{δ+} ratio of 0.33, (c) Pt₁ at 100% with a Pt₁⁰/Pt₁^{δ+} ratio of 1.78, (d) 2D clusters and 3D ensembles, and (e) 3D ensembles and particles. (D) In situ FT-IR spectra for Pt/Zn(Al)O with Pt present as Pt₁²⁺, Pt₁ at 100% with a Pt₁⁰/Pt₁^{δ+} ratio of 0.33, and Pt₁ at 100% with a Pt₁⁰/Pt₁^{δ+} ratio of 1.78 with (a) styrene adsorbed, (b) pyrrolidine adsorbed following styrene adsorption, (c) pyrrolidine adsorbed, and (d) styrene adsorbed following pyrrolidine adsorption. Styrene and pyrrolidine activation modes are also given with red: O²⁻; blue-gray: Zn²⁺; magenta: Al³⁺; green: Pt₁⁰ or Pt₁^{δ+}; aqua: Pt₁⁰; gray: C; white: H; blue: N.

cm⁻¹) predominates over Pt₁^{δ+} (the band at 2070 cm⁻¹) in quantity, and the ratio of Pt₁⁰ to Pt₁^{δ+} was determined as 2.12

or 1.78. More atomic-scale Pt₁ are observed to be located at lattice Zn(Al) sites from the HAADF-STEM images (Figure

S9), accounting for the higher ratio of Pt_1^0 to $Pt_1^{\delta+}$. The EPR signals assigned to Pt_1 ($g = 1.971$) are more visible for 0.11 wt % Pt/Zn(Al)O-100% Pt_1 (Figure 2B), consistent with higher Pt_1 sites than 0.11 wt % Pt/Zn(Al)O. For 0.11 wt % Pt/Zn(Al)O-re-14% Pt_1 or 0.11 wt % Pt/Zn(Al)O-18% Pt_1 , the predominant Pt_1 is $Pt_1^{\delta+}$ (the band at 2070 cm^{-1}), and the bridge-bound CO on the Pt ensemble support (the band at 1945 cm^{-1}) is visibly observed (Figure 2A). For 0.11 wt % Pt/Zn(Al)O-0 Pt_1 , only 2D Pt clusters (the band at 1995 cm^{-1}) and Pt ensembles (the band at 1945 cm^{-1}) are observed (Figure 2A), and no EPR signal assigned to Pt_1 ($g = 1.971$) is observed (Figure 2B) because of the formation of a Pt–Pt bond at 100%. In the addition of styrene and pyrrolidine (Table 1) catalyzed by 0.11 wt % Pt/Zn(Al)O-re-100% Pt_1 and 0.11 wt % Pt/Zn(Al)O-re-14% Pt_1 (Table 1, entries 8 and 9), both from the post-treatment of 0.11 wt % Pt/Zn(Al)O, it is found that an increased Pt_1 ratio affords a higher TON (Table 1, entry 8 vs 3), while a decreased Pt_1 ratio affords a lower TON (Table 1, entry 9 vs 3), further demonstrating that Pt_1 are the active sites. Similar catalytic results are observed with 0.11 wt % Pt/Zn(Al)O-100% Pt_1 and 0.11 wt % Pt/Zn(Al)O-18% Pt_1 , in which Pt dispersion has been tailored directly in the preparation (Table 1, entries 10 and 11). An increased Pt_1 ratio affords a higher TON (Table 1, entry 10 vs 3), while a decreased Pt_1 ratio affords a lower TON (Table 1, entry 11 vs 3); 100% Pt–Pt affords no TON (Table 1, entry 12), further confirming that Pt_1 are the active sites for hydroamination of styrene with pyrrolidine, and the Pt sites in Pt–Pt linkage, including 2D clusters and 3D ensembles, are not active for this reaction.

2.2.2. Pt_1 Sites for Markovnikov or Anti-Markovnikov C–N Formation. In the addition of styrene and pyrrolidine (Table 1), 0.01 wt % Pt/Zn(Al)O (Table 1, entry 1) affords a selectivity of 90% to Markovnikov product, which is not surprising because previous studies have demonstrated Pt(II) complexes are effective in the Markovnikov hydroamination,^{30,31} and even the $PhICl_2$ -oxidized heterogeneous Pt nanoparticles catalyzed the Markovnikov addition of nitrogen nucleophiles to alkynes and allenes.²⁴ With the emergence of Pt_1^0 (0.05 wt % Pt/Zn(Al)O), the C–N addition turns out anti-Markovnikov (Table 1, entry 2) product, affording a selectivity of 55% to anti-Markovnikov addition. With a further increase in Pt_1^0 ratio, the selectivity to anti-Markovnikov product increases, while Markovnikov selectivity decreases (Table 1, entries 3–6). An anti-Markovnikov selectivity of 85% or above (Table 1, entries 2–6) has been achieved on 0.11, 0.30, 1.01, and 2.12 wt % Pt/Zn(Al)O, indicating that Pt_1^0 sites contribute to anti-Markovnikov selectivity.

Compared to 0.11 wt % Pt/Zn(Al)O, the increase in the ratio of Pt_1^0 (0.11 wt % Pt/Zn(Al)O-re-100% Pt_1 and 0.11 wt % Pt/Zn(Al)O-100% Pt_1) results in an increase in the selectivity to anti-Markovnikov (Table 1, entries 8 and 10 vs 3), while the increase in the ratio of $Pt_1^{\delta+}$ (0.11 wt % Pt/Zn(Al)O-re-14% Pt_1 and 0.11 wt % Pt/Zn(Al)O-18% Pt_1) causes an increase in the selectivity to Markovnikov (Table 1, entries 9 and 11 vs 3). The results confirm that the Pt_1^0 site accounts for the anti-Markovnikov selectivity, while the $Pt_1^{\delta+}$ site accounts for the Markovnikov selectivity.

2.3. Pt_1 -Catalyzed Mechanism for Anti-Markovnikov C–N Formation. It is interesting, as can be seen from Table 1, that the TON based on the atomic-scale Pt (TON_{Pt}) is not a simple increase with increasing ratio of Pt_1^0 sites, but displays first an increase and then a decrease with the increase of Pt_1^0 /

$Pt_1^{\delta+}$ ratio. Thus, a cooperating catalysis between $Pt_1^{\delta+}$ and Pt_1^0 could be deduced for the anti-Markovnikov C–N addition.

2.3.1. The Role of Pt_1 Sites in C=C and N–H Activation. To clarify the role of $Pt_1^{\delta+}$ and Pt_1^0 in the anti-Markovnikov C–N addition, in situ FT-IR spectra of styrene and pyrrolidine adsorption–desorption have been recorded, respectively (Figure 3A and B). No bands can be found on Zn(Al)O (Figure 3A and B, a), suggesting the support has no active sites for styrene or pyrrolidine adsorption. For the adsorption of styrene (Figure 3A), the C–H stretching vibrations of the benzene ring⁶⁰ at 3030 and 3080 cm^{-1} , observed for each Pt/Zn(Al)O here, suggest that both Pt_1 and Pt–Pt sites can adsorb styrene. The π -bonding of styrene^{49,61,62} to Pt_1 is observed at 1619 cm^{-1} on Pt_1^{2+} , blue-shifting to 1622 cm^{-1} on $Pt_1^{\delta+}$ and to 1630 cm^{-1} on Pt_1^0 , suggesting that the interactions between Pt_1 and C=C becomes weaker with increasing electron density of Pt_1 sites (Figure 3A, b–f). The C–H stretching vibrations of CH=CH₂ (at 3045 and 3090 cm^{-1})⁶² also demonstrate the π -bonding of styrene to Pt_1 . The bands assigned to CH=CH₂ around 3090, 3045, and 1605–1642 cm^{-1} are not observed when no Pt_1 but only Pt–Pt sites (including 2D clusters, 3D ensembles, and particles) exist (Figure 3A, g and h). The di- σ -bonded adsorption of styrene^{63–65} is accordingly observed at 2855, 2910, and 2952 cm^{-1} when Pt–Pt appears and becomes predominating with the increase in Pt–Pt ratio (Figure 3A, e–h). Relating the catalytic results in Table 1 to styrene adsorption, it can be deduced that the styrene activation in π -bonding mode on Pt_1 is responsible for the C–N addition, whether on Pt_1^{2+} , $Pt_1^{\delta+}$, or Pt_1^0 .

In the FT-IR spectra of pyrrolidine adsorption (Figure 3B), the CH₂ stretching vibrations of amine (at 2970 and 2880 cm^{-1}),⁶⁶ observed for each Pt/Zn(Al)O, suggest that both of Pt_1 and Pt–Pt sites have the ability to adsorb amine. The N–H stretching vibration^{67,68} is observed at 3220 cm^{-1} on electron-deficient Pt_1^{2+} or $Pt_1^{\delta+}$ (Figure 3B, b and c), but disappears when Pt_1^0 increases (Figure 3B, d–f) and blue shifts to 3230 cm^{-1} on Pt–Pt sites (Figure 3B, g and h). The results show that in the activation of pyrrolidine, N–H cleavage occurs on Pt_1^0 while N–H is reserved on the electron-deficient Pt_1^{2+} or $Pt_1^{\delta+}$, or Pt–Pt sites. The EPR spectra for Pt/Zn(Al)O with pyrrolidine adsorbed (Figure 3C) confirm the observations in FT-IR spectra. The signal of an unpaired electron at $g = 1.971$ disappears for Pt_1^0 and does not change for $Pt_1^{\delta+}$ or Pt_1^{2+} or Pt–Pt sites after pyrrolidine adsorption, suggesting pyrrolidine is adsorbed with the N radical on Pt_1^0 sites, affording an electrophilic N center, while with N electron pairs on Pt_1^{2+} or $Pt_1^{\delta+}$ or Pt–Pt sites, affording a nucleophilic N center. It is consistent with the theoretical prediction^{69,70} that Pt^0 sites can adsorb and activate the amines to be electrophilic. Relating the catalytic results in Table 1 to pyrrolidine adsorption, it can be deduced that the pyrrolidine activation with N–H cleavage on Pt_1^0 , other than Pt_1^{2+} , $Pt_1^{\delta+}$, or Pt–Pt, is responsible for the anti-Markovnikov C–N addition.

The FT-IR spectra of styrene and pyrrolidine competitive adsorption on either Pt_1^{2+} or the Pt_1 with varied $Pt_1^0/Pt_1^{\delta+}$ ratio (Figure 3D) show that π -bonded styrene on Pt_1 (Figure 3D, a) can be completely replaced by pyrrolidine (Figure 3D, b), and the pyrrolidine adsorbed on Pt_1 sites (Figure 3D, c) can be partially replaced by styrene (Figure 3D, d), suggesting both the styrene and pyrrolidine are adsorbed on Pt_1 sites dynamically. The pyrrolidine on Pt_1^{2+} is easily replaced by styrene while the replacement becomes harder with increasing

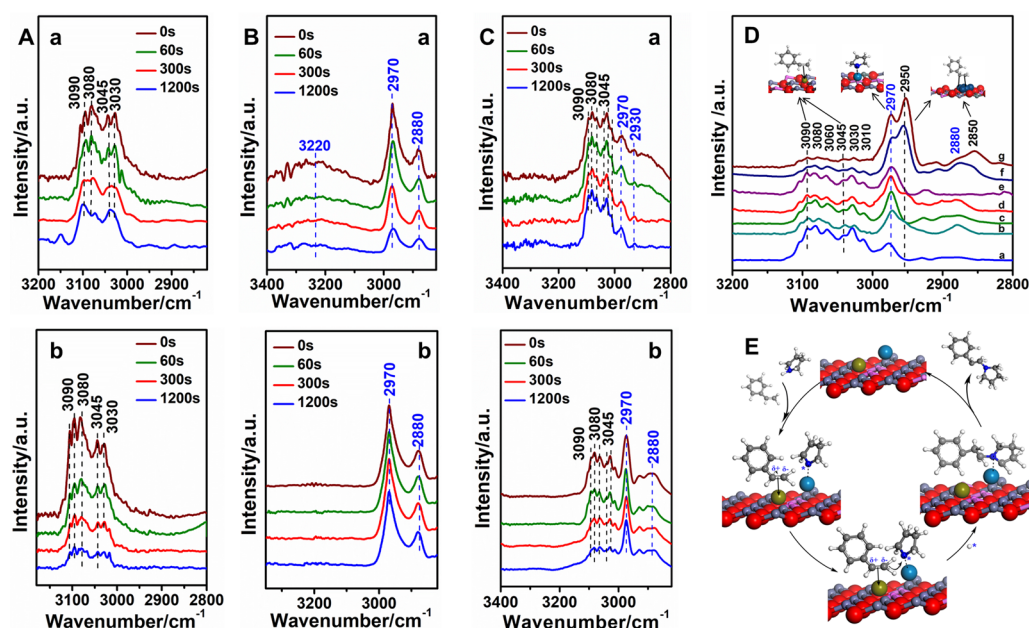


Figure 4. In situ FT-IR spectra of (A) styrene, (B) pyrrolidine, and (C) their mixture with the time-dependent desorption on Pt/Zn(Al)O with Pt present as Pt₁ at 100% with a Pt₁⁰/Pt₁^{δ+} ratio of (a) 0.33 and (b) 1.78. (D) In situ FT-IR spectra for the coadsorption of pyrrolidine and styrene on Pt/Zn(Al)O with Pt present as (a) Pt₁ at 100% with a Pt₁⁰/Pt₁^{δ+} ratio of 0.33, (b) Pt₁ at 76% with a Pt₁⁰/Pt₁^{δ+} ratio of 0.89, (c) Pt₁ at 100% with a Pt₁⁰/Pt₁^{δ+} ratio of 1.78, (d) Pt₁ at 47% with a Pt₁⁰/Pt₁^{δ+} ratio of 2.03, (e) Pt₁ at 100% with a Pt₁⁰/Pt₁^{δ+} ratio of 2.12, (f) Pt₁ at 38% with a Pt₁⁰/Pt₁^{δ+} ratio of 2.45, and (g) Pt₁ at 30% with a Pt₁⁰/Pt₁^{δ+} ratio of 3.55. (E) Possible reaction pathway for the anti-Markovnikov C–N formation: red: O²⁻; blue-gray: Zn²⁺; magenta: Al³⁺; green: Pt₁^{δ+}; aqua: Pt₁⁰; gray: C; white: H; blue: N.

Pt₁⁰/Pt₁^{δ+} ratio, suggesting that nucleophilic N–H adsorbed on Pt₁²⁺ or Pt₁^{δ+} sites can be easily replaced, but the electrophilic N adsorbed on Pt₁⁰ cannot be replaced by styrene. Thus, it could be deduced that the nucleophilic N–H and C=C on Pt₁²⁺ or Pt₁^{δ+} contribute to the Markovnikov addition, while the C=C activated on Pt₁^{δ+} sites and the electrophilic N activated on Pt₁⁰ sites are proposed to be responsible for the anti-Markovnikov C–N formation.

2.3.2. Cooperating Catalysis between Pt₁^{δ+} and Pt₁⁰. To figure out the cooperating catalysis between Pt₁⁰ and Pt₁^{δ+} in the anti-Markovnikov C–N formation, the in situ FT-IR spectra of the styrene and pyrrolidine adsorption–desorption on Pt₁ have been recorded (Figure 4A–C). The styrene is difficult to desorb from the Pt/Zn(Al)O with Pt₁^{δ+} dominant (Figure 4A, a) and becomes easier with increasing Pt₁⁰ (Figure 4A, b), and pyrrolidine is easy to desorb from the Pt/Zn(Al)O with Pt₁^{δ+} dominant (Figure 4B, a) and becomes more difficult with increasing Pt₁⁰ (Figure 4B, b). The results confirm that C=C is preferred to be activated on Pt₁^{δ+} and pyrrolidine on Pt₁⁰ sites. In the coadsorption (Figure 4C), the styrene adsorption predominates over pyrrolidine on the Pt/Zn(Al)O with Pt₁^{δ+} dominant (Figure 4C, a), while pyrrolidine adsorption predominates over styrene on the Pt/Zn(Al)O with Pt₁⁰ dominant (Figure 4C, b). But either styrene or pyrrolidine adsorption hardly changes in the desorption (Figure 4C), indicative of the simultaneous activation of styrene and pyrrolidine. The coadsorption on the Pt/Zn(Al)O with varied Pt dispersion (Figure 4D) displays a decrease in styrene adsorption and meanwhile an increase in pyrrolidine adsorption with the increase of Pt₁⁰/Pt₁^{δ+} ratio, confirming the simultaneous activation of styrene and pyrrolidine. In the simultaneous activation of styrene with pyrrolidine (Figure S10), C=C is π-bonded to Pt₁^{δ+} (1621–1622 cm⁻¹) rather than Pt₁⁰ sites (1630 cm⁻¹). In the FT-IR spectra of styrene

and pyrrolidine coadsorption on Pt–Pt sites (Figure S11), no pyrrolidine adsorption but di-σ-bonded styrene is observed, suggesting the di-σ-bonded adsorption of styrene on Pt–Pt sites is not only inactive itself but also so strong as to prohibit the activation of pyrrolidine.

Therefore, a possible mechanism for the anti-Markovnikov C–N formation is proposed (Figure 4E). The styrene is initially π-bonded to Pt₁^{δ+} sites and the pyrrolidine adsorbed on Pt₁⁰ sites with N–H cleavage. Then, it is the attack of activated C=C on Pt₁^{δ+} sites to the electrophilic N on Pt₁⁰ sites that is responsible for the anti-Markovnikov C–N formation. Higher TON_{Pt1} has been achieved with a controlled Pt₁⁰/Pt₁^{δ+} ratio of ca. 2 (Table 1, entry 4 or 10), meaning a cooperating catalysis between Pt₁^{δ+} and Pt₁⁰ for C–N formation. Two Pt₁⁰ sites are needed for the Pt–N and Pt–H formation, while one Pt₁^{δ+} for the C=C activation, although it is a pity that no Pt–H bands are observed in the FT-IR spectra.

2.4. Reusability. The spent catalyst (0.11 wt % Pt/Zn(Al)O–re-100% Pt₁) has been recycled (Figure 5) simply by centrifugation and reused without any regeneration. Almost

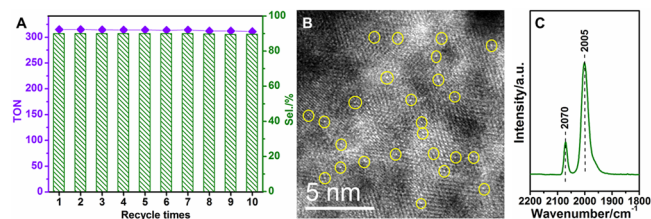


Figure 5. (A) Recycling of 0.11 wt % Pt/Zn(Al)O–re-100% Pt₁ for the addition of styrene and pyrrolidine. (B) HAADF-STEM images and (C) the in situ FT-IR spectra of CO adsorbed on 0.11 wt % Pt/Zn(Al)O–re-100% Pt₁ after 10 runs.

Table 2. Olefin and Amine Scope for Anti-Markovnikov C–N Addition on 0.11 wt % Pt/Zn(Al)O-re-100% Pt₁^a

anti-Markovnikov (a-M) Markovnikov (M)

Entry	R ₁	R ₂	R ₃	Product	Sel./ %		TON ^b
					a-M	M	
1	n-Hex	H	R ₂ , R ₃ =c-Bu		83	17	61
2	Ph	H	Ph		91	9	296
3	Ph	Et	n-Bu		88	12	168
4	Ph	H	n-pentyl		86	14	83
5	4-NCC ₆ H ₄	H	Ph		90	10	325
6	4-MeC ₆ H ₄	H	Ph		91	9	288
7	4-MeOC ₆ H ₄	H	Ph		93	7	257
8	n-Hex	H	Ph		85	15	72

^aReaction conditions: styrene (0.6 mmol), pyrrolidine (0.3 mmol), catalysts (exposed Pt = 0.067 mol %), and solvent (isopropanol 1.5 mL) in a Schlenk tube, $T = 60\text{ }^{\circ}\text{C}$, $t = 8\text{ h}$. ^bTON was calculated based on the number of surface Pt sites. The number of surface Pt sites was estimated from the Pt dispersion (D_{Pt} in Table S1).

no decrease in TON (>310) and the selectivity for anti-Markovnikov (90%) are observed in 10 runs (Figure 5A). Correspondingly, the atomic dispersion of Pt is well retained in the catalysis, according to the HAADF-STEM image (Figure 5B). According to the in situ FT-IR spectra of CO adsorption (Figure 5C), for the used 0.11 wt % Pt/Zn(Al)O-re-100% Pt₁⁰ (the band at 2005 cm⁻¹) predominates over Pt₁^{δ+} (the band at 2070 cm⁻¹) in quantity, and the ratio of Pt₁⁰ to Pt₁^{δ+} was determined as 2.35, being maintained at a similar level to the fresh 0.11 wt % Pt/Zn(Al)O-re-100% Pt₁ (a Pt₁⁰/Pt₁^{δ+} ratio of 2.12).

2.5. Substrate Scope and Tolerance. The substrate scope and tolerance were then explored (Table 2). In addition to styrene (Table 1), aliphatic olefin (*n*-octene here) can also carry out anti-Markovnikov hydroamination with pyrrolidine, affording an anti-Markovnikov selectivity of 83% and TON of 61 (Table 2, entry 1). In addition to pyrrolidine (Table 1), aromatic aniline, aliphatic linear secondary amines (*n*-ethyl-*n*-butylamine here), and aliphatic linear primary amines (*n*-pentylamine here) can carry out hydroamination with styrene, affording an anti-Markovnikov selectivity of 86–91% and a TON of 83–296 (Table 2, entries 2–4). Substituted styrene (cyano, methyl, methoxy substituents) and aliphatic olefin (*n*-octene here) can all carry out anti-Markovnikov hydroamination with aromatic aniline, which is more challenging

than with pyrrolidine, affording an anti-Markovnikov selectivity of 85–93% and TON of 72–325 (Table 2, entries 5–8). An intramolecular C–N addition of *N*-4-hexen-1-yl-benzenemethanamine to anti-Markovnikov product has also been successfully accomplished in a selectivity of 87% and a TON of 155. It is a pity that the C–N addition of aliphatic olefins with aliphatic linear amines (*n*-pentylamine with *n*-octene, *n*-hexene, 2-methylpentene, 1-methylhexene, or 4-nitrilehexene; *n*-octene with *N*-ethyl-*n*-butylamine, *N*-ethyl-*n*-hexylamine, or *N*-methylcyclohexylamine here), which has not been achieved in previous report,^{22,23} was also not available with this catalyst. According to the literature,^{22,23} the benzene ring serves as an electron-withdrawing ligand for the C=C or NH moiety. Thus, the electrophilic N activated by the Pt₁⁰ can be more electrophilic with the benzene ring, and nucleophilic β-C activated by Pt₁^{δ+} can be more nucleophilic. Without an electron-withdrawing aromatic moiety, aliphatic linear olefins or aliphatic linear amines are more difficult to be activated.

3. CONCLUSIONS

This work has demonstrated successful C–N addition via hydroamination of olefins with amines on supported atomic-scale Pt. Atomic Pt sites have been identified as the active sites by tailoring Pt dispersion. Relating the chemical state of atomic Pt to the activity and regioselectivity in intermolecular

hydroamination, it has been found that Pt_1^{2+} is active for Markovnikov C–N formation, while atomic Pt ($\text{Pt}_1^{\delta+}$ and Pt_1^0) contributes to anti-Markovnikov C–N formation. A TON of up to 331 and a selectivity of 92% to anti-Markovnikov has been afforded over atomic Pt. A cooperating catalysis between $\text{Pt}_1^{\delta+}$ and Pt_1^0 in the anti-Markovnikov C–N formation of styrene and pyrrolidine has been revealed by EPR spectra and in situ FT-IR spectra of adsorption–desorption of styrene and/or pyrrolidine. The Pt_1^0 sites are revealed to activate N for the attack of $\text{Pt}_1^{\delta+}$ -activated C=C. This strategy is also effective for the anti-Markovnikov addition of aromatic olefins with aromatic/aliphatic amines, aromatic/aliphatic olefins with aromatic amines, and linear aliphatic olefins with secondary aliphatic amines.

4. EXPERIMENTAL SECTION

4.1. Preparation. ZnAl-LDHs. ZnAl-LDHs were prepared in a pH-constant co-precipitation method. Typically, $\text{Zn}(\text{NO}_3)_2 \cdot 6\text{H}_2\text{O}$ (0.04 mol) and $\text{Al}(\text{NO}_3)_3 \cdot 9\text{H}_2\text{O}$ (0.02 mol) in 100 mL of deionized water and a solution of NaOH (0.08 mol) and Na_2CO_3 (0.01 mol) in 100 mL of deionized water were simultaneously added drop by drop to a round-bottomed flask with 300 mL of deionized water under constant pH (10.0), and then the mixture was aged at 60 °C for 12 h under stirring. The solid was filtrated, washed thoroughly with deionized water until the filtrate was neutral, and dried at 60 °C in an air oven overnight.

$[\text{Pt}(\text{NH}_3)_4]^{2+}/\text{ZnAl-LDHs}$. Pt was loaded on ZnAl-LDHs by the incipient wetness impregnation method. Typically, 1.5 g of ZnAl-LDHs was impregnated with 1.5 mL of aqueous solution containing 270 μmol of platinum tetraammine (PTA, $[\text{Pt}(\text{NH}_3)_4]^{2+}$), giving 3.54 wt % Pt loading on ZnAl-LDHs. In the same method, $[\text{Pt}(\text{NH}_3)_4]^{2+}/\text{ZnAl-LDHs}$ in Pt loadings of 0.008, 0.04, 0.07, 0.09, 0.22, 0.73, and 1.50 wt % were prepared with aqueous solution containing 0.6, 3.0, 5.2, 7.2, 15.7, 53.2, and 112.0 μmol of PTA.

$\text{Pt}/\text{Zn}(\text{Al})\text{O}$. Pt-loaded ZnAl-LDO was produced by calcination of $[\text{Pt}(\text{NH}_3)_4]^{2+}/\text{ZnAl-LDHs}$ under a reduction atmosphere. Typically, $[\text{Pt}(\text{NH}_3)_4]^{2+}/\text{ZnAl-LDHs}$ in varying Pt loadings was calcined at 550 °C in hydrogen flow for 2 h with the temperature programmed from room temperature to 550 °C at a rate of 5 °C min^{-1} . The samples are denoted as 0.01 wt % Pt/Zn(Al)O, 0.05 wt % Pt/Zn(Al)O, 0.11 wt % Pt/Zn(Al)O, 0.30 wt % Pt/Zn(Al)O, 2.12 wt % Pt/Zn(Al)O, and 5.05 wt % Pt/Zn(Al)O, according to the inductively coupled plasma emission spectrometer (ICP-ES) determination.

0.11 wt % Pt/Zn(Al)O-re-100% Pt₁. Pt/Zn(Al)O (0.11 wt %) was first treated in air at 550 °C for 2 h, cooled to room temperature, and then reduced at 280 °C in H_2 for 1 h. The temperature was programmed from room temperature to 550 or 280 °C at a rate of 5 °C min^{-1} .

The 0.11 wt % Pt/Zn(Al)O-re-14% Pt₁, 0.11 wt % Pt/Zn(Al)O-100% Pt₁, 0.11 wt % Pt/Zn(Al)O-18% Pt₁, and 0.11 wt % Pt/Zn(Al)O-0Pt₁ were also prepared (see details in SI 2.1).

4.2. Characterizations. The powder XRD measurements were performed on a Rigaku XRD-6000 diffractometer, using Cu K α radiation ($\lambda = 0.15418$ nm) at 40 kV and 30 mA, with a scanning rate of 5° min^{-1} . The quantitative analysis for Pt was performed on a Shimadzu ICPS-7500 ICP-ES. Before measurements, 5 mg of the sample was dissolved by nitric acid and transferred to a volumetric flask, diluted to 10 mL with deionized water. HAADF-STEM images were taken on a JEM-ARM 200F electron microscope capable of subångström resolution. The samples for STEM measurements were pretreated in absolute ethanol under ultrasonic conditions before depositing onto a copper grid coated with a thin holey carbon film. The EPR spectra were measured on a Bruker A300-10/12 EPR spectrometer (110 K, 9650 MHz, X band). The samples, as-prepared or pretreated with 0.5 vol % pyrrolidine/Ar flow at 60 °C, were saved in Ar and transferred to the analysis quartz tube without exposure to air.

Pt dispersion was measured on a Micrometric ChemiSorb 2750 chemisorption instrument with a thermal conductivity detector by the HOT method and the procedure reported in the literature (see details in SI 2.2.1). In situ FT-IR of CO adsorption in transmission mode was recorded on a Nicolet 380 model (Thermo Electron Corporation) equipped with a high-temperature cell fitted with BaF_2 windows and an MCT-A detector, with a resolution of 2 cm^{-1} using 64 scans (see details in SI 2.2.2). In situ FT-IR of styrene and pyrrolidine adsorption in transmission mode was recorded on a Nicolet 380 model (Thermo Electron Corporation) equipped with a high-temperature cell fitted with BaF_2 windows and an MCT-A detector, with a resolution of 2 cm^{-1} using 64 scans (see details in SI 2.2.3).

4.3. Catalytic Test. The hydroamination reaction was conducted in a sealed glass tube. A 0.3 mmol amount of amine, 0.6 mmol of alkene, and catalyst (exposed Pt = 0.067 mol %) were added into the reactor tube with 1.5 mL of isopropanol. After stirring for 8 h at 60 °C, the catalyst was separated by centrifugation and the liquid phase was analyzed on the Shimadzu GC-2014C equipped with a DB-5 capillary column in line with a FID.

$$\text{Selectivity} = [n_{\text{product}} / (n_{\text{amine,initial}} - n_{\text{amine,left}})] \times 100\% \quad (1)$$

$$\text{TON} = (n_{\text{amine,initial}} - n_{\text{amine,left}}) / (n_{\text{Pt}} \times D_{\text{Pt}}) \quad (2)$$

$$\text{TON}_{\text{Pt1}} = (n_{\text{amine,initial}} - n_{\text{amine,left}}) / (n_{\text{Pt}} \times D_{\text{Pt}} \times \text{ratio}_{\text{Pt1}}) \quad (3)$$

In formulas 2 and 3, D_{Pt} was determined by the HOT method with the TPR-2920. In formula 3, $\text{ratio}_{\text{Pt1}}$ was estimated from HAADF-STEM images.

Purification by Kugelrohr distillation yielded the product as a colorless oil. ^1H NMR and ^{13}C NMR spectra were recorded on a Bruker DRX 400 (400 MHz for ^1H , 100 MHz for ^{13}C) at room temperature. High-resolution mass spectra (HRMS) were obtained on a XEVO-G2QTOF spectrometer and were reported as m/z (relative intensity). As for the reaction, the spent catalyst was recovered by centrifugation, thoroughly washed with isopropanol, and then reused as catalyst for the hydroamination reaction.

■ ASSOCIATED CONTENT

Supporting Information

The Supporting Information is available free of charge at <https://pubs.acs.org/doi/10.1021/jacs.0c02997>.

Experimental details and characterizations (PDF)

■ AUTHOR INFORMATION

Corresponding Author

Jing He – State Key Laboratory of Chemical Resource Engineering & Beijing Advanced Innovation Center for Soft Matter Science and Engineering, Beijing University of Chemical Technology, Beijing 100029, People's Republic of China; orcid.org/0000-0002-2940-6675; Phone: +86-10-64425280; Email: jinghe@263.net.cn, hejing@mail.buct.edu.cn; Fax: +86-10-64425385

Authors

Xiaodan Ma – State Key Laboratory of Chemical Resource Engineering & Beijing Advanced Innovation Center for Soft Matter Science and Engineering, Beijing University of Chemical Technology, Beijing 100029, People's Republic of China
Zhe An – State Key Laboratory of Chemical Resource Engineering & Beijing Advanced Innovation Center for Soft Matter Science and Engineering, Beijing University of Chemical Technology, Beijing 100029, People's Republic of China
Hongyan Song – State Key Laboratory of Chemical Resource Engineering & Beijing Advanced Innovation Center for Soft

Matter Science and Engineering, Beijing University of Chemical Technology, Beijing 100029, People's Republic of China

Xin Shu – State Key Laboratory of Chemical Resource Engineering & Beijing Advanced Innovation Center for Soft Matter Science and Engineering, Beijing University of Chemical Technology, Beijing 100029, People's Republic of China

Xu Xiang – State Key Laboratory of Chemical Resource Engineering & Beijing Advanced Innovation Center for Soft Matter Science and Engineering, Beijing University of Chemical Technology, Beijing 100029, People's Republic of China;

orcid.org/0000-0003-1089-6210

Complete contact information is available at:
<https://pubs.acs.org/10.1021/jacs.0c02997>

Notes

The authors declare no competing financial interest.

ACKNOWLEDGMENTS

Financial support from NSFC of China (21521005, 91634120), National Key R&D Program of China (2017YFA0206804), and the Fundamental Research Funds for the Central Universities (XK1802-6) are gratefully acknowledged.

REFERENCES

- (1) Chen, A.; Holt-Hindle, P. Platinum-Based Nanostructured Materials: Synthesis, Properties, and Applications. *Chem. Rev.* **2010**, *110*, 3767–3804.
- (2) Yu, W.; Porosoff, M. D.; Chen, J. G. Review of Pt-Based Bimetallic Catalysis: From Model Surfaces to Supported Catalysts. *Chem. Rev.* **2012**, *112*, 5780–5817.
- (3) Wang, Y.; Zhao, N.; Fang, B.; Li, H.; Bi, X. T.; Wang, H. Carbon-Supported Pt-Based Alloy Electrocatalysts for the Oxygen Reduction Reaction in Polymer Electrolyte Membrane Fuel Cells: Particle Size, Shape, and Composition Manipulation and Their Impact to Activity. *Chem. Rev.* **2015**, *115*, 3433–3467.
- (4) Hernández-Pichardo, M. L.; Macías-Salinas, R. Modeling the *n*-Hexane Isomerization over Iron Promoted Pt/WO_x-ZrO₂ Catalysts Using Artificial Neural Networks. *Ind. Eng. Chem. Res.* **2016**, *55*, 8883–8889.
- (5) O'Driscoll, Á.; Curtin, T.; Hernández, W. Y.; Voort, P. V. D.; Leahy, J. J. Hydrogenation of Furfural with a Pt–Sn Catalyst: The Suitability to Sustainable Industrial Application. *Org. Process Res. Dev.* **2016**, *20*, 1917–1929.
- (6) Sattler, J. J. H. B.; Ruiz-Martinez, J.; Santillan-Jimenez, E.; Weckhuysen, B. M. Catalytic Dehydrogenation of Light Alkanes on Metals and Metal Oxides. *Chem. Rev.* **2014**, *114*, 10613–10653.
- (7) Zanchet, D.; Santos, J. B. O.; Damyanova, S.; Gallo, J. M. R.; Bueno, J. M. C. Toward Understanding Metal-Catalyzed Ethanol Reforming. *ACS Catal.* **2015**, *5*, 3841–3863.
- (8) Ciriminna, R.; Pandarus, V.; Bèland, F.; Xu, Y.; Pagliaro, M. Heterogeneously Catalyzed Alcohol Oxidation for the Fine Chemical Industry. *Org. Process Res. Dev.* **2015**, *19*, 1554–1558.
- (9) Sheng, H.; Ma, H.; Qian, W.; Fei, N.; Zhang, H.; Ying, W. Platinum–Copper Bimetallic-Modified Nanoprism Mordenite for Carbonylation of Dimethyl Ether. *Energy Fuels* **2019**, *33*, 10159–10166.
- (10) An, K.; Alayoglu, S.; Musselwhite, N.; Na, K.; Somorjai, G. A. Designed Catalysts from Pt Nanoparticles Supported on Macroporous Oxides for Selective Isomerization of *n*-Hexane. *J. Am. Chem. Soc.* **2014**, *136*, 6830–6833.
- (11) Sun, M.; Liu, J.; Song, C.; Ogata, Y.; Rao, H.; Zhao, X.; Xu, H.; Chen, Y. Different Reaction Mechanisms of Ammonia Oxidation Reaction on Pt/Al₂O₃ and Pt/CeZrO₂ with Various Pt States. *ACS Appl. Mater. Interfaces* **2019**, *11*, 23102–23111.

- (12) Garcia, A. C.; Kolb, M. J.; Sanchez, C. N.; Vos, J.; Birdja, Y. Y.; Kwon, Y.; Tremiliosi-Filho, G.; Koper, M. T. M. Strong Impact of Platinum Surface Structure on Primary and Secondary Alcohol Oxidation during Electro-Oxidation of Glycerol. *ACS Catal.* **2016**, *6*, 4491–4500.

- (13) Liu, L.; Corma, A. Metal Catalysts for Heterogeneous Catalysis: From Single Atoms to Nanoclusters and Nanoparticles. *Chem. Rev.* **2018**, *118*, 4981–5079.

- (14) Qiao, B.; Wang, A.; Yang, X.; Allard, L. F.; Jiang, Z.; Cui, Y.; Liu, J.; Li, J.; Zhang, T. Single-atom catalysis of CO oxidation using Pt₁/FeO_x. *Nat. Chem.* **2011**, *3*, 634–641.

- (15) Wei, H.; Liu, X.; Wang, A.; Zhang, L.; Qiao, B.; Yang, X.; Huang, Y.; Miao, S.; Liu, J.; Zhang, T. FeO_x-supported platinum single-atom and pseudo-single-atom catalysts for chemoselective hydrogenation of functionalized nitroarenes. *Nat. Commun.* **2014**, *5*, 5634–5641.

- (16) Li, H.; Wang, L.; Dai, Y.; Pu, Z.; Lao, Z.; Chen, Y.; Wang, M.; Zheng, X.; Zhu, J.; Zhang, W.; Si, R.; Ma, C.; Zeng, J. Synergetic interaction between neighbouring platinum monomers in CO₂ hydrogenation. *Nat. Nanotechnol.* **2018**, *13*, 411–418.

- (17) Xie, P.; Pu, T.; Nie, A.; Hwang, S.; Purdy, S. C.; Yu, W.; Su, D.; Miller, J. T.; Wang, C. Nanoceria-Supported Single-Atom Platinum Catalysts for Direct Methane Conversion. *ACS Catal.* **2018**, *8*, 4044–4048.

- (18) Corbet, J.-P.; Mignani, G. Selected Patented Cross-Coupling Reaction Technologies. *Chem. Rev.* **2006**, *106*, 2651–2710.

- (19) Evano, G.; Blanchard, N.; Toumi, M. Copper-Mediated Coupling Reactions and Their Applications in Natural Products and Designed Biomolecules Synthesis. *Chem. Rev.* **2008**, *108*, 3054–3131.

- (20) Ruiz-Castillo, P.; Buchwald, S. L. Applications of Palladium-Catalyzed C–N Cross-Coupling Reactions. *Chem. Rev.* **2016**, *116*, 12564–12649.

- (21) Cho, S.; Kim, J.; Kwak, J.; Chang, S. Recent advances in the transition metal-catalyzed twofold oxidative C–H bond activation strategy for C–C and C–N bond formation. *Chem. Soc. Rev.* **2011**, *40*, 5068–5083.

- (22) Huang, L.; Arndt, M.; Gooßen, K.; Heydt, H.; Gooßen, L. J. Late Transition Metal-Catalyzed Hydroamination and Hydroamidation. *Chem. Rev.* **2015**, *115*, 2596–2697.

- (23) Müller, T. E.; Hultsch, K. C.; Yus, M.; Foubelo, F.; Tada, M. Hydroamination: Direct Addition of Amines to Alkenes and Alkynes. *Chem. Rev.* **2008**, *108*, 3795–3892.

- (24) Brunet, J. J.; Cadena, M.; Chu, N. C.; Diallo, O.; Jacob, K.; Mothes, E. The First Platinum-Catalyzed Hydroamination of Ethylene. *Organometallics* **2004**, *23*, 1264–1268.

- (25) Witham, C. A.; Huang, W.; Tsung, C.; Kuhn, J. N.; Somorjai, G. A.; Toste, F. D. Converting homogeneous to heterogeneous in electrophilic catalysis using monodisperse metal nanoparticles. *Nat. Chem.* **2010**, *2*, 36–41.

- (26) Panunzi, A.; Renzi, A. D.; Palumbo, R.; Paiaro, G. Addition Reactions on Coordinated Olefinic Ligands. II. The Reaction between Amines and Monoolefins Coordinated in *cis*-Dichloro (olefin) (f-phosphine) platinum (II) Complexes. *J. Am. Chem. Soc.* **1969**, *91*, 3879–3883.

- (27) Wang, X.; Widenhoefer, R. A. Platinum-Catalyzed Intermolecular Hydroamination of Unactivated Olefins with Carboxamides. *Organometallics* **2004**, *23*, 1649–1651.

- (28) Bender, C. F.; Widenhoefer, R. A. Platinum-Catalyzed Intramolecular Hydroamination of Unactivated Olefins with Secondary Alkylamines. *J. Am. Chem. Soc.* **2005**, *127*, 1070–1071.

- (29) Rodriguez-Zubiri, M.; Anguille, S.; Brunet, J.-J. Intermolecular hydroamination of non-activated alkenes catalyzed by Pt(II) or Pt(IV)-*n*-Bu₄PX (X = Cl, Br, I) systems: Key effect of the halide anion. *J. Mol. Catal. A: Chem.* **2007**, *271*, 145–150.

- (30) Rodriguez-Zubiri, M.; Anguille, S.; Brunet, J.-J.; Daran, J.-C. Pt-catalysed intermolecular hydroamination of non-activated olefins using a novel family of catalysts: Arbuzov-type phosphorus metal complexes. *J. Mol. Catal. A: Chem.* **2013**, *379*, 103–111.

- (31) Hoove, J. M.; DiPasquale, A.; Mayer, J. M.; Michael, F. E. Platinum-Catalyzed Intramolecular Hydrohydrozination: Evidence for Alkene Insertion into a Pt-N Bond. *J. Am. Chem. Soc.* **2010**, *132*, 5043–5053.
- (32) Beller, M.; Trauthwein, H.; Eichberger, M.; Breindl, C.; Herwig, J.; Müller, T. E.; Thiel, O. R. The First Rhodium-Catalyzed Anti-Markovnikov Hydroamination: Studies on Hydroamination and Oxidative Amination of Aromatic Olefins. *Chem. - Eur. J.* **1999**, *5*, 1306–1319.
- (33) Timmerman, J. C.; Robertson, B. D.; Widenhoefer, R. A. Gold-Catalyzed Intermolecular Anti-Markovnikov Hydroamination of Alkylidenecyclopropanes. *Angew. Chem., Int. Ed.* **2015**, *54*, 2251–2254.
- (34) Utsunomiya, M.; Hartwig, J. F. Ruthenium-Catalyzed Anti-Markovnikov Hydroamination of Vinylarenes. *J. Am. Chem. Soc.* **2004**, *126*, 2702–2703.
- (35) Takaya, J.; Hartwig, J. F. Mechanistic Studies of Ruthenium-Catalyzed Anti-Markovnikov Hydroamination of Vinylarenes: Intermediates and Evidence for Catalysis through π -Arene Complexes. *J. Am. Chem. Soc.* **2005**, *127*, 5756–5757.
- (36) Musacchio, A. J.; Lainhart, B. C.; Zhang, X.; Naguib, S. G.; Sherwood, T. C.; Knowles, R. R. Catalytic intermolecular hydroaminations of unactivated olefins with secondary alkyl amines. *Science* **2017**, *355*, 727–730.
- (37) Zhu, Q.; Graff, D. E.; Knowles, R. R. Intermolecular Anti-Markovnikov Hydroamination of Unactivated Alkenes with Sulfonamides Enabled by Proton-Coupled Electron Transfer. *J. Am. Chem. Soc.* **2018**, *140*, 741–747.
- (38) Brunet, J. J.; Commenges, G.; Neibecker, D.; Philippot, K. Rhodium-catalysed hydroamination-hydroarylation of norbornene with aniline, toluidines or diphenylamine. *J. Organomet. Chem.* **1994**, *469*, 221–228.
- (39) Burling, S.; Field, L. D.; Messerle, B. A.; Turner, P. Intramolecular Hydroamination Catalyzed by Cationic Rhodium and Iridium Complexes with Bidentate Nitrogen-Donor Ligands. *Organometallics* **2004**, *23*, 1714–1721.
- (40) Zhang, J.; Yang, C.; He, C. Gold(I)-Catalyzed Intra- and Intermolecular Hydroamination of Unactivated Olefins. *J. Am. Chem. Soc.* **2006**, *128*, 1798–1799.
- (41) Liu, X. Y.; Li, C. H.; Che, C. M. Phosphine Gold(I)-Catalyzed Hydroamination of Alkenes under Thermal and Microwave-Assisted Conditions. *Org. Lett.* **2006**, *8*, 2707–2710.
- (42) Uchimaru, Y. N–H activation vs. C–H activation: ruthenium-catalysed regioselective hydroamination of alkynes and hydroarylation of an alkene with N-methylaniline. *Chem. Commun.* **1999**, 1133–1134.
- (43) Yi, C. S.; Yun, S. Y. Ruthenium-Catalyzed Intermolecular Coupling Reactions of Arylamines with Ethylene and 1,3-Dienes: Mechanistic Insight on Hydroamination vs ortho-C–H Bond Activation. *Org. Lett.* **2005**, *7*, 2181–2183.
- (44) Sevov, C. S.; Zhou, J.; Hartwig, J. F. Iridium-Catalyzed, Intermolecular Hydroamination of Unactivated Alkenes with Indoles. *J. Am. Chem. Soc.* **2014**, *136* (8), 3200–3207.
- (45) Cowan, R. L.; Troglor, W. C. Syntheses, Reactions, and Molecular Structures of trans-Hydrido(phenylamido)bis(triethylphosphine)platinum(II) and trans-Hydrido phenoxobis(triethylphosphine)platinum(II). *J. Am. Chem. Soc.* **1989**, *111*, 4750–4761.
- (46) Cowan, R. L.; Troglor, W. C. Regioselective Insertion of Acrylonitrile Into the Pt-N Bond of Hydrido(phenylamido) bis(triethylphosphine)-platinum(II), A Model Step for Olefin Amination. *Organometallics* **1987**, *6*, 2451–2453.
- (47) Ma, X.; An, Z.; Zhu, Y.; Wang, W.; He, J. Pseudo-single-atom Platinum Induced by the Promoter Confined in Brucite-like Lattice for Catalytic Reforming. *ChemCatChem* **2016**, *8*, 1773–1777.
- (48) Zhu, Y.; An, Z.; He, J. Single-atom and small-cluster Pt induced by Sn (IV) sites confined in an LDH lattice for catalytic reforming. *J. Catal.* **2016**, *341*, 44–54.
- (49) Zhu, Y.; An, Z.; Song, H.; Xiang, X.; Yan, W.; He, J. Lattice-Confined Sn (IV/II) Stabilizing Raft-Like Pt Clusters: High Selectivity and Durability in Propane Dehydrogenation. *ACS Catal.* **2017**, *7*, 6973–6978.
- (50) Tichit, D.; Das, N.; Coq, B.; Durand, R. Preparation of Zr-Containing Layered Double Hydroxides and Characterization of the Acido-Basic Properties of Their Mixed Oxides. *Chem. Mater.* **2002**, *14*, 1530–1538.
- (51) Pushparaj, S. S. C.; Forano, C.; Prevot, V.; Lipton, A. S.; Rees, G. J.; Hanna, J. V.; Nielsen, U. G. How the Method of Synthesis Governs the Local and Global Structure of Zinc Aluminum Layered Double Hydroxides. *J. Phys. Chem. C* **2015**, *119*, 27695–27707.
- (52) Zhu, X.; Cho, H.; Pasupong, M.; Regalbutto, J. R. Charge-Enhanced Dry Impregnation: A Simple Way to Improve the Preparation of Supported Metal Catalysts. *ACS Catal.* **2013**, *3*, 625–630.
- (53) Benson, J. E.; Boudart, M. Hydrogen-Oxygen Titration Method for the Measurement of Supported Platinum Surface Areas. *J. Catal.* **1965**, *4*, 704–710.
- (54) Nie, L.; Mei, D.; Xiong, H.; Peng, B.; Ren, Z.; Hernandez, X. I. P.; DeLaRiva, A.; Wang, M.; Engelhard, M. H.; Kovarik, L.; Datsy, A. K.; Wang, Y. Activation of surface lattice oxygen in single-atom Pt/CeO₂ for low-temperature CO oxidation. *Science* **2017**, *358*, 1419–1423.
- (55) Pozdnyakova, O.; Teschner, D.; Wootsch, A.; Kröhnert, J.; Steinhauer, B.; Sauer, H.; Toth, L.; Jentoft, F. C.; Knop-Gericke, A.; Paál, Z.; Schlögl, R. Preferential CO oxidation in hydrogen (PROX) on ceria-supported catalysts, part I: Oxidation state and surface species on Pt/CeO₂ under reaction conditions. *J. Catal.* **2006**, *237*, 1–16.
- (56) Pozdnyakova, O.; Teschner, D.; Wootsch, A.; Kröhnert, J.; Steinhauer, B.; Sauer, H.; Toth, L.; Jentoft, F. C.; Knop-Gericke, A.; Paál, Z.; Schlögl, R. Preferential CO oxidation in hydrogen (PROX) on ceria-supported catalysts, part II: Oxidation states and surface species on Pd/CeO₂ under reaction conditions, suggested reaction mechanism. *J. Catal.* **2006**, *237*, 17–28.
- (57) Yu, B.; Zhu, C.; Gan, F.; Huang, Y. Electron spin resonance properties of ZnO microcrystallites. *Mater. Lett.* **1998**, *33*, 247–250.
- (58) Chang, T.; Tanaka, Y.; Ishikawa, R.; Toyoura, K.; Matsunaga, K.; Matsunaga, Y.; Shibata, N. Direct Imaging of Pt Single Atoms Adsorbed on TiO₂ (110) Surfaces. *Nano Lett.* **2014**, *14*, 134–138.
- (59) Matsubu, J. C.; Yang, V. N.; Christopher, P. Isolated Metal Active Site Concentration and Stability Control Catalytic CO₂ Reduction Selectivity. *J. Am. Chem. Soc.* **2015**, *137*, 3076–3084.
- (60) Liu, Y.; Wu, W.; Guan, Y.; Ying, P.; Li, C. FT-IR Spectroscopic Study of the Oxidation of Chlorobenzene over Mn-Based Catalyst. *Langmuir* **2002**, *18*, 6229–6232.
- (61) Jiang, F.; Zeng, L.; Li, S.; Liu, G.; Wang, S.; Gong, J. Propane Dehydrogenation over Pt/TiO₂-Al₂O₃ Catalysts. *ACS Catal.* **2015**, *5*, 438–447.
- (62) Yu, J.; Wang, R.; Ren, S.; Sun, X.; Chen, C.; Ge, Q.; Fang, W.; Zhang, J.; Xu, H.; Su, D. S. The Unique Role of CaO in Stabilizing the Pt/Al₂O₃ Catalyst for the Dehydrogenation of Cyclohexane. *ChemCatChem* **2012**, *4*, 1376–1381.
- (63) Amakawa, K.; Wrabetz, S.; Kröhnert, J.; Tzolova-Müller, G.; Schlögl, R.; Trunschke, A. In Situ Generation of Active Sites in Olefin Metathesis. *J. Am. Chem. Soc.* **2012**, *134*, 11462–11473.
- (64) Cremer, P. S.; Su, X.; Shen, Y. R.; Somorjai, G. A. Ethylene Hydrogenation on Pt(111) Monitored in Situ at High Pressures Using Sum Frequency Generation. *J. Am. Chem. Soc.* **1996**, *118*, 2942–2949.
- (65) Cremer, P. S.; Su, X.; Shen, Y. R.; Somorjai, G. A. Hydrogenation and Dehydrogenation of Propylene on Pt(111) Studied by Sum Frequency Generation from UHV to Atmospheric Pressure. *J. Am. Chem. Soc.* **1996**, *118*, 16302–16309.
- (66) Jackson, P.; Robinson, K.; Puxty, G.; Attalla, M. In situ Fourier Transform-Infrared (FT-IR) analysis of carbon dioxide absorption and desorption in amine solutions. *Energy Procedia* **2009**, *1*, 985–994.

(67) Chang, M. C.; Tanaka, J. FT-IR study for hydroxyapatite/collagen nanocomposite cross-linked by glutaraldehyde. *Biomaterials* **2002**, *23*, 4811–4818.

(68) Amoresa, J. M. G.; Escribano, V. S.; Ramisb, G.; Buscab, G. An FT-IR study of ammonia adsorption and oxidation over anatase-supported metal oxides. *Appl. Catal., B* **1997**, *13*, 45–58.

(69) Tsipis, C. A.; Kefalidis, C. E. How Efficient Are the Hydrido-Bridged Diplatinum Catalysts in the Hydrosilylation, Hydrocyanation, and Hydroamination of Alkynes: A Theoretical Analysis of the Catalytic Cycles Employing Electronic Structure Calculation Methods. *Organometallics* **2006**, *25*, 1696–1706.

(70) Tsipis, C. A.; Kefalidis, C. E. Hydrosilylation, hydrocyanation, and hydroamination of ethane catalyzed by bis(hydrido-bridged)-diplatinum complexes: Added insight and predictions from theory. *J. Organomet. Chem.* **2007**, *692*, 5245–5255.